Research Article | Vol. 31, No. 10 / 8 May 2023 / Optics Express 15836

Optics EXPRESS

Enhanced ultrathin ultraviolet detector based on a diamond metasurface and aluminum reflector

JIAJING FENG,[1,2] ZHONGZHU LIANG,[1,2,3,4] XIAOYAN SHI,[3] XIQING ZHANG,[3] DEJIA MENG,[1,5] RUI DAI,[3] SHOUTAO ZHANG,[3] YAN JIA,[3] NINGTE YAN,[3] SIXUAN LI,[3] AND ZIHAN WANG[3]

[1] *Changchun Institute of Optics, Fine Mechanics and Physics, Chinese Academy of Sciences, Changchun, Jilin, 130033, China*
[2] *University of the Chinese Academy of Sciences, Beijing 100049, China*
[3] *Center for Advanced Optoelectronic Functional Materials Research and Key Laboratory of UV Light-Emitting Materials and Technology of Ministry of Education, College of Physics, Northeast Normal University, Changchun 130024, China*
[4] *liangzz@nenu.edu.cn*
[5] *djmeng@sklao.ac.cn*

Abstract: Metasurface is a kind of sub-wavelength artificial electromagnetic structure, which can resonate with the electric field and magnetic field of the incident light, promote the interaction between light and matter, and has great application value and potential in the fields of sensing, imaging, and photoelectric detection. Most of the metasurface-enhanced ultraviolet detectors reported so far are metal metasurfaces, which have serious ohmic losses, and studies on the use of all-dielectric metasurface-enhanced ultraviolet detectors are rare. The multilayer structure of the diamond metasurface-gallium oxide active layer-silica insulating layer-aluminum reflective layer was theoretically designed and numerically simulated. In the case of gallium oxide thickness of 20 nm, the absorption rate of more than 95% at the working wavelength of 200-220 nm is realized, and the working wavelength can be adjusted by changing the structural parameters. The proposed structure has the characteristics of polarization insensitivity and incidence angle insensitivity. This work has great potential in the fields of ultraviolet detection, imaging, and communications.

1. Introduction

Ultraviolet detectors are widely used in important fields such as space communications, missile guidance, discharge detection, ozone detection, and medical applications [1–4]. Ultraviolet detectors are gradually developing towards high integration, high performance, multi-dimensional detection, and miniaturization [5–7]. The development of modern science and technology puts forward higher requirements for the performance of ultraviolet detectors. However, high-quality semiconductor films are difficult to grow [8], and the light capture ability of traditional ultraviolet detectors is weak. For photon detectors, their detection performance is limited by the absorption law exp(–αd), where α is the absorption coefficient and d is the thickness of the absorbing layer. Therefore, to improve the performance of the detector, on the one hand, it is necessary to optimize the structural parameters to obtain a high absorption coefficient, on the other hand, to obtain a high absorption rate, sufficient semiconductor thickness is usually required to improve quantum efficiency. Nevertheless, the larger d increases the carrier crossing time and response time, the material growth process is stressful, and the product cost is high, which is not conducive to the integration and miniaturization of photonic detectors development. Therefore, seeking new ways to improve the absorption rate of semiconductors, reduce the reflectivity, and reduce the thickness of the absorption layer while maintaining a high absorption rate is of great significance to improve the responsiveness and ease of integration of ultraviolet detectors.

#488265 https://doi.org/10.1364/OE.488265
Journal © 2023 Received 22 Feb 2023; revised 8 Apr 2023; accepted 9 Apr 2023; published 26 Apr 2023

Many metasurface-based enhanced photodetectors have been reported, and studies have shown that metasurface is an effective way to enhance photodetectors [9]. Metasurface is a kind of sub-wavelength artificial electromagnetic structure, which can resonate with the electric field and magnetic field of the incident light and can break through the limitations of certain apparent natural laws and produce electromagnetic responses that do not exist in nature, to obtain functions that are not available in natural materials, such as negative refractive index, perfect absorber and metalenses [10].

Metasurfaces have great application value and potential in the fields of sensing, imaging, and photoelectric detection. Many applications of metasurfaces operating in the ultraviolet range have been reported. Cheng et al. demonstrate high-performance metasurface optical components formed of hafnium oxide that operate at ultraviolet wavelengths [11], enabling diverse applications including lithography, imaging, spectroscopy, and quantum information processing. Lei Chen et al. propose an Ultraviolet sensing metasurface for programmable electromagnetic scattering field manipulation [12], the spatial distribution of sensing light by sensors can be used to determine the electromagnetic field and connect sensing optical information with the microwave field. Not only that, ultraviolet metasurfaces are also widely used in many fields such as circular dichroism spectroscopy [13,14], high-resolution imaging [15,16], structured light generation [17,18], and hologram projection [19,20].

Metal surface plasmon nanoparticles or metasurfaces have been widely used to enhance the performance of photonic detectors [21–28]. For example, Ruifan Tang et al. [29]. proposed improved Ga_2O_3 solar-blind photodetectors decorated by Rh metal nanoparticles. Dark current was greatly reduced and the detective was highly improved. Metal discrete particles or polymer arrays excited local surface plasmon resonance enhances the electric field and promotes the interaction between light and optoelectronic materials, but it also introduces severe ohmic losses, especially in the ultraviolet band. Moreover, rare metals are too expensive, which is not conducive to cost saving and promotion. In addition, all-dielectric metasurface resonators supporting Mie resonance have also been used to generate near-field enhancement and facilitate light collection [30–37]. However, at present, the working wavelengths of photon detectors based on all-dielectric metasurface are mainly concentrated in the visible and infrared bands, while research on all-dielectric metasurface-enhanced ultraviolet detectors is rarely reported. Therefore, to obtain a low-loss, efficient metasurface that works in the ultraviolet band, it is necessary to select the appropriate dielectric material. In addition, the gallium oxide-based ultraviolet detectors currently reported still have the characteristics of low responsivity and slow response speed [38], and it is difficult to deposit high-quality thin films [39]. A larger thickness is required to obtain better performance [40,41]. Under the trend of miniaturization and integration of photonic devices, the contradiction between a high absorption rate and small thickness needs to be solved urgently.

Given the need for a high absorption rate and small absorption layer thickness of ultraviolet detector, this paper proposes a multilayer structure of diamond resonator-gallium oxide active layer-silicon oxide insulating layer-aluminum reflective layer. The proposed metasurface structure is a two-dimensional periodic diamond nanopillar array, which greatly improved the absorption supported by Mie resonance in the ultraviolet band. For gallium oxide films at 20 nm, the absorption rate at the wavelength of 205 nm is increased from 30% to above 90%. The ideal responsivity under 0.5 mW incident optical power irradiation increased from 0.08 A/W to 0.15 A/W, and the carrier generation rate on the surface of the gallium oxide film after the introduction of metasurface increased to 6 times that of the monolayer gallium oxide film. At the same time, the low loss characteristics of diamond avoid the ohmic loss caused by metal plasmon resonators. The introduced aluminum metal film has high reflectivity in the ultraviolet band, which reduces the transmittance of incident light and increases the optical path so that the required thickness of the gallium oxide layer to obtain a large absorption rate is greatly reduced. In addition, the influence of geometric parameters on the absorption characteristics is studied, and the designed metasurface has the characteristics of polarization insensitivity and incidence angle insensitivity.

2. Structural design

The structure of the metasurface-based ultraviolet detector is shown in Fig. 1. The metasurface consists of periodically arranged nanocylinders. Diamond is selected as the metasurface material because it has a high refractive index (n~2.6), supports Mie resonance, and is lossless below the wavelength of 240 nm. In addition, there are mature technologies for fabricating high-quality nanoscale diamond structures [42,43]. The active layer of the detector adopts gallium oxide, which is a wide bandgap semiconductor material commonly used in ultraviolet detection. Silica is an insulating layer and metallic aluminum is a reflector. The diamond resonator in the upper layer has a radius of R = 50 nm, a height of H = 35 nm, and a period of P = 120 nm. The thickness of the gallium oxide film is 20 nm, and the thickness of the silica film is 20 nm.

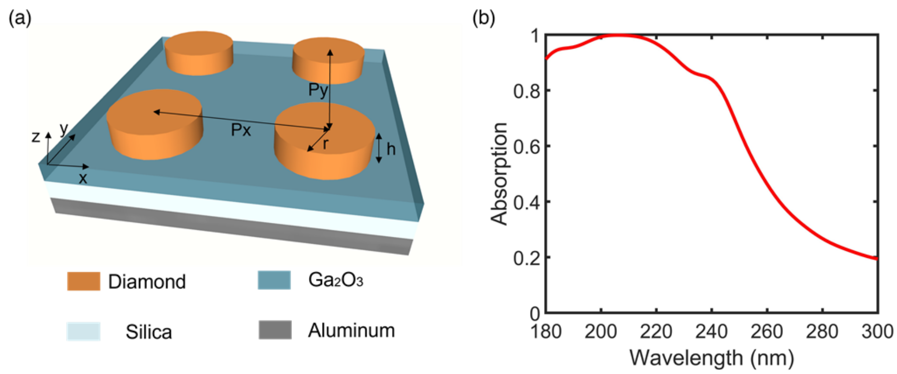

Fig. 1. (a) Schematic diagram of gallium oxide ultraviolet detector based on diamond metasurface and (b) its absorption spectrum.

The time-domain finite difference method is used to simulate and calculate the optical response and performance of metasurface ultraviolet detectors. The simulation was performed using the Lumerical FDTD solution. The incident light is set to linearly polarized light occurring in the negative direction of the Z axis with a wavelength range of 180-300 nm. The boundary conditions in the X and Y-axis directions are set as periodic boundary conditions, and the Z-axis direction uses perfectly matched layer boundary conditions. Two frequency-domain field profile monitors are placed above the diamond array and below the Al film to detect the reflectance and transmittance of the system, respectively. The absorption spectrum is defined as A = 1-R-T, where R and T are simulated results of structural reflectance and transmittance, respectively. An optical generation rate analysis object was placed covering the volume of the gallium oxide film. The optical generation can be calculated by this analysis object by assuming that each absorbed photon generates one electron-hole pair.

optical constants of materials used in the calculation were extracted from the data reported [44–47]. The optical constants of the materials are depicted in Fig. 2, where the solid line represents the refractive index n of the material and the dashed line represents the extinction coefficient k of the material.

Gallium oxide films can be grown using various techniques, such as chemical vapor deposition (CVD) [48], molecular beam epitaxy (MBE) [49], pulsed laser deposition (PLD) [50], and atomic layer deposition (ALD) [51]. Currently, synthetic diamonds are prepared by either a high-pressure high-temperature (HPHT) or a CVD process [52]. To obtain high-pure, low-cost and reproducible diamond, the CVD process is a better choice. Diamond can be bonded with Ga_2O_3 by van der

Optics EXPRESS

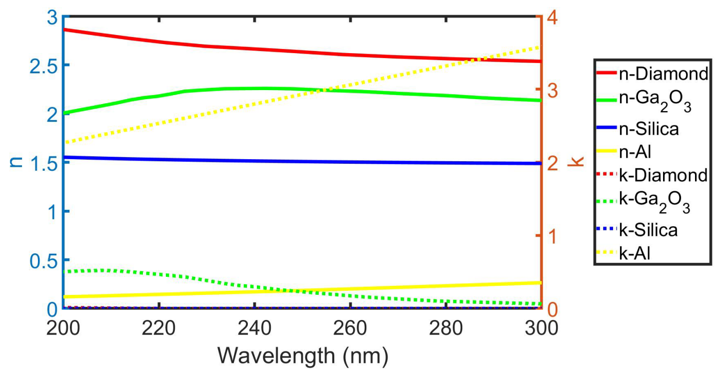

Fig. 2. Refractive index n and the extinction coefficient k as a function of wavelength for Diamond, Ga2O3, Silica, and Al.

Waals interaction. Ga_2O_3 can be deposited onto single-crystal diamond substrates by ALD. Many studies on gallium oxide bonded to diamond have been reported [52–56]. We believe that our design is practical.

3. Results discussion

3.1. Optical response and physical mechanisms

The optical response of metasurface-based detectors under different conditions was studied, as shown in Fig. 3(a). The absorption, reflectance, and transmission spectra under different conditions are shown in Fig. 3(b)-(d).

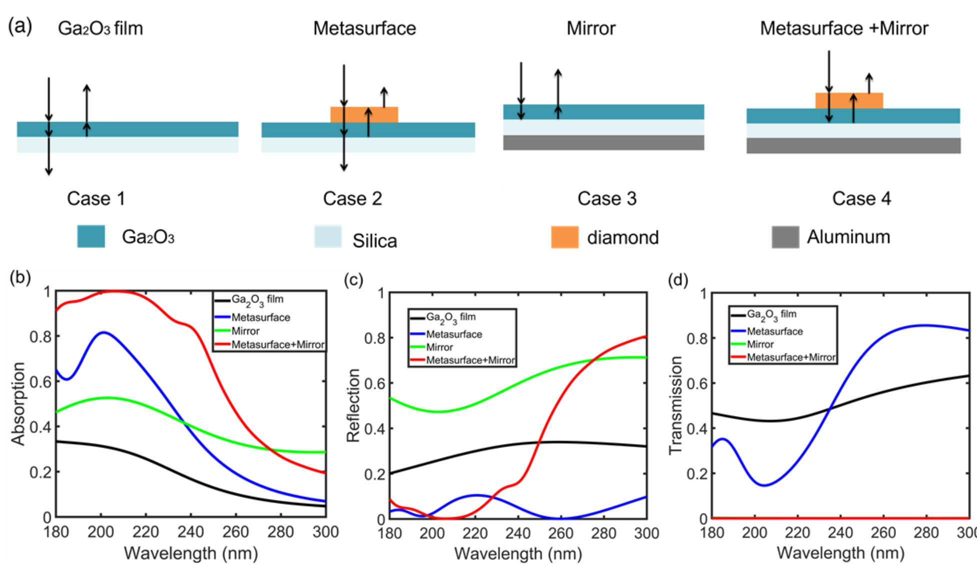

Fig. 3. (a)Absorption enhancement mechanisms in different situations; (b)-(d) Absorption, reflection, and transmission spectra under different conditions.

First, we consider the gallium oxide semiconductor film (Fig. 3(a) case 1), when the light incident on the gallium oxide film, the incident light is reflected vertically at the interface between air and gallium oxide, part of the light is absorbed by the gallium oxide film, and the unabsorbed

Optics EXPRESS

light passes through the sample. This results in a decrease in the efficiency of gallium oxide films. The effect of gallium oxide film thickness on the absorption rate was studied, and it can be seen from Fig. 4 that the absorption rate gradually decreases as the thickness of gallium oxide film decreases. Therefore, to increase the absorption rate, a sufficiently thick gallium oxide film is required, but at the same time, it also increases the volume of the device, which is not easy to miniaturize and integrate the detector and increases the carrier crossing time, decreasing sensitivity. Therefore, for detectors with a gallium oxide thickness of 20 nm, to improve the absorption rate of the detector, we introduced metasurfaces and mirrors.

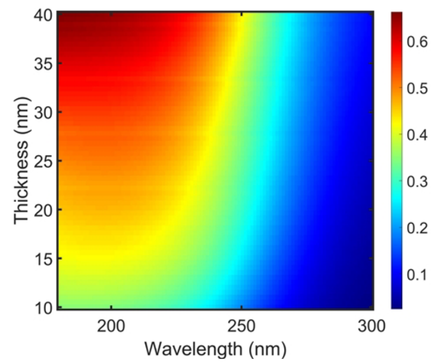

Fig. 4. Absorption rate vs. thickness of gallium oxide film.

With the introduction of diamond metasurfaces (case 2), we simulate the reflection and transmission spectra of the structure, as shown in Fig. 3(c) and (d). Compared with the simple gallium oxide film, the reflectivity, and transmittance of the structure are reduced at the wavelength of 200 nm-220 nm, resulting in a significant increase in the absorption rate. There are two resonance reflection dips around 197 and 260 nm in the reflection spectra of the metasurface, as shown in the blue curve of Fig. 3(c). To explore the cause of the reflection dips, we calculated the electromagnetic field distribution of the metasurface at the wavelength of 197 nm and 260 nm, as shown in Fig. 5, the electric field distribution has the distribution characteristics of dipoles.

The magnetic field is mainly concentrated in the diamond resonator and the active layer of gallium oxide, and the local enhancement of the electromagnetic field promotes the interaction between incident light and gallium oxide. The resonance mode appearing at the wavelength of 197 nm is derived from an electric dipole mode (ED), while the mode around 260 nm is caused by a magnetic dipole mode (MD). Owing to reflection inhibition, the absorption increased. When the resonance wavelength of MD and ED approaches each other, Huygens' metasurfaces [57] will appear. The backward scattering would be suppressed, which means the reflection of the metasurface would be reduced. This phenomenon is also known as the Kerker condition.

In addition, a considerable portion of the transmitted light in case 1 is not absorbed, which can be further enhanced by introducing a metal mirror (case 3). A 50 nm-thick aluminum film is deposited under the silica substrate, which drastically reduces the transmittance, to almost 0. However, the reflectivity of the structure has increased compared to case 1, and the overall absorption rate has increased slightly, which is due to the reflection of the aluminum film. The distance ultraviolet light interacts with gallium oxide films increase, and during reflection, a part of the energy of light is absorbed and converted into photogenerated carriers.

In summary, for a layer of gallium oxide film, when only the diamond metasurface is introduced, the reflectivity and transmittance are suppressed at a specific wavelength, and the absorption rate is greatly increased according to the formula A = 1-R-T. However, because the transmittance cannot be completely suppressed to 0, the absorption rate cannot approach 1 indefinitely. When only a mirror is introduced, the transmittance of the structure is almost 0, but the reflectivity

Optics EXPRESS

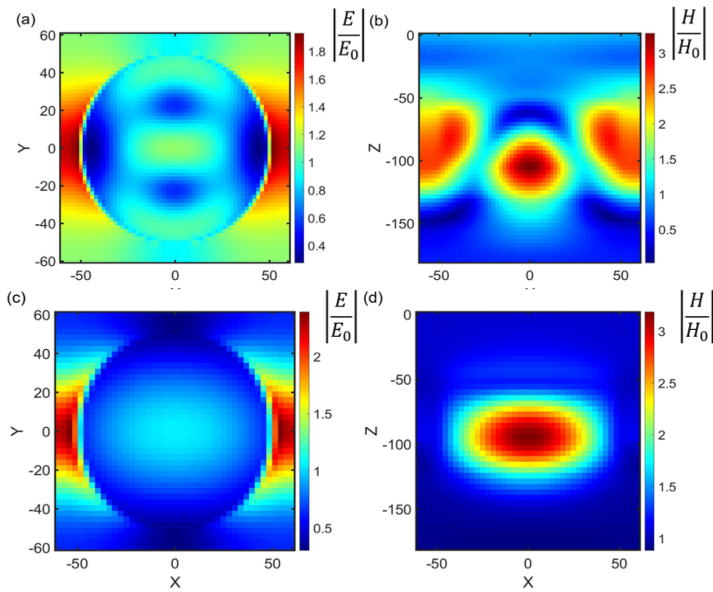

Fig. 5. (a) xOy plane electric field distribution and (b) xOz plane magnetic field distribution at the wavelength of 197 nm; (c) xOy plane electric field distribution and (d) xOz plane magnetic field distribution at the wavelength of 260 nm.

increases. Therefore, consider case 4, i.e. the simultaneous introduction of diamond metasurfaces and aluminum-metal mirrors to gallium oxide films.

The absorption curve of the detector in case 4 can be seen as the result of a combination of metasurface and mirror, as shown in Fig. 3(b). The proposed structure has an absorption rate of more than 90% in the wavelength range of 200-220 nm, and the absorption rate at 205 nm tends to be close to 1. As shown in Fig. 3(d), the thin aluminum thin film still makes the transmittance of the structure almost 0, but in the wavelength range of 200-220 nm, the reflectivity introduced by the mirror is suppressed by the diamond metasurface. The reflectivity also tends to be 0, as shown in Fig. 3(c).

Mie resonator combined with reflector achieving perfect absorber has been realized [36,31]. When the MD mode and ED mode of the Mie resonance approach to coincide, the backscattering of the metasurface is suppressed. However, due to the existence of the metal mirror, the light cannot pass through the structure. According to the formula A = 1-R-T, almost all of the energy of the incident light is absorbed by the device.

Figure 6 shows the absorptance of the proposed structure and a 200 nm gallium oxide film under the same conditions. It can be seen that the proposed structure has higher absorptance than 200 nm pure gallium oxide film at a wavelength of 180-240 nm. This shows that the proposed structure can greatly improve the absorption rate of the gallium oxide ultraviolet detector, and at the same time reduce the required semiconductor film thickness, which is beneficial to the miniaturization and integration of ultraviolet detectors.

The carrier generation rate is a parameter that characterizes the efficiency of incident light interacting with the active layer to produce photogenerated carriers. The rate of generation of electron-hole pairs through photon absorption is known as the “optical generation rate”. The optical generation rate is usually denoted by G(x). The actual number of electron-hole pairs generated by the absorbed photons is described by the quantum efficiency, η, of the process. Now,

Optics EXPRESS

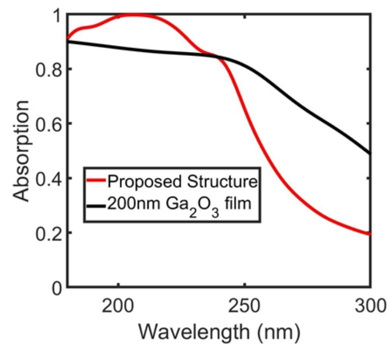

Fig. 6. Absorption curve of the proposed structure and 200 nm gallium oxide film under the same conditions.

the optical generation rate is given by:

$$G(x) = \eta\alpha I(x) = \eta\alpha I_0 \exp(-\alpha x) \tag{1}$$

where α is the absorption coefficient, I(x) is the Light intensity (photons/cm^{2}s) absorbed at the distance x. α and η depend on the wavelength. So to calculate the generation rate in a device, we must integrate

$$G(x) = \int_{\lambda_1}^{\lambda_2} \eta(\lambda)\alpha(\lambda)I_0 \exp[-\alpha(\lambda)x]dx \tag{2}$$

We simulated carrier generation at a wavelength of 205 nm with a source intensity of 0.5 mW, as shown in Fig. 7. After the introduction of the diamond metasurface, the distribution map of carrier generation rate in the plane of xOy on the surface of gallium oxide is similar to the distribution of the electric field. The maximum carrier generation of the proposed device is up to 9.6×10^{25} charge pairs/m^3/s, while the maximum carrier generation without the metasurface is only 1.53×10^{25} charge pairs/m^3/s. The maximum carrier generation rate is about 6 times that of no metasurface.

Figure 8 shows the ideal responsivity curve of a gallium oxide detector under 0.5 mW incident optical power irradiation. The ideal responsiveness can be calculated by the formula below:

$$R = \frac{I_{ph}}{P}; I_{ph} = J_{\mathrm{sc}} \times S \tag{3}$$

where I_{ph} is the photocurrent, J_{sc} is the ideal photocurrent normalized to the surface area, obtained by the simulation results, P is the incident optical power, and S is the illumination area. It can be seen from the responsivity curve that the enhancement trend is similar to the absorption curve, and the maximum responsivity is significantly enhanced from 0.08 A/W to 0.15A/W. The above electrical indicators further verify the effect of diamond metasurface on enhancing ultraviolet detectors.

3.2. Influence of geometric parameters

We examined the influence of metasurface geometry parameters on detector absorption. Figure 9 shows the absorption at different radii, altitudes, and periods. With the increase of the radius of the diamond nanopillar, the absorption peak is slightly redshifted, and the change in the aspect ratio of the diamond nanopillar makes the resonance wavelength of Mie's resonance redshift. The change in height has a great influence on absorption. It is necessary to select the appropriate period to obtain the required absorption rate. Based on the above results and analysis, the

Optics EXPRESS

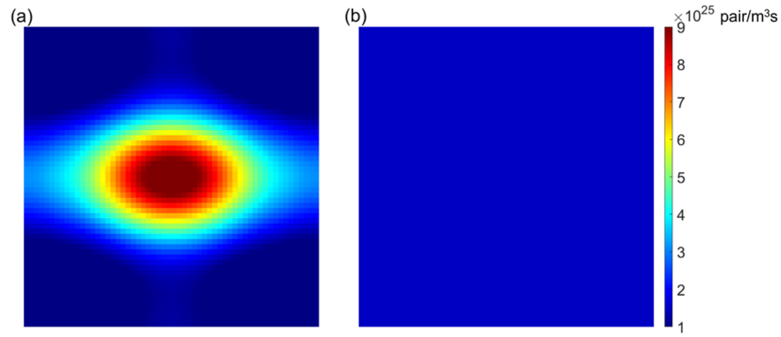

Fig. 7. Comparison of carrier generation rates of (a)gallium oxide film with diamond metasurface and (b) without diamond metasurface at 205 nm.

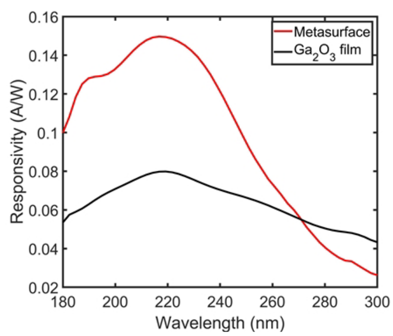

Fig. 8. Responsivity of single gallium oxide film and diamond metasurfaces

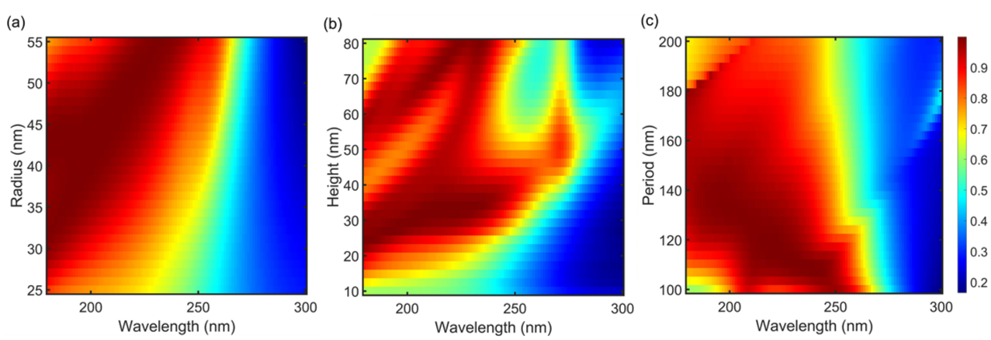

Fig. 9. Effects of different (a) radius, (b) height, and (c) period on absorption.

absorption can be adjusted by changing the geometric parameters of the diamond metasurface to meet different practical application needs.

To characterize the effect of the polarization angle and incidence angle of incident light on the absorption of the detector. We examined the absorption rate of the detector with an incident polarization angle from 0 to 90 degrees, and the results are shown in Fig. 10(a). The absorption rate hardly changes with the angle of incidence polarization because the periodic structure of the metasurface is centrally symmetrical. In many applications, it is crucial to have a material or device that can absorb radiation over a wide range of angles. For example, in solar energy systems, large-angle absorbers can capture more sunlight throughout the day, leading to higher energy efficiency. In thermal management, large-angle absorbers can efficiently dissipate heat from electronic devices, leading to better performance and longer lifetimes. It's necessary to study the incident angle's effect on the absorption properties of our design. In the case of linear polarized light incidence, the incidence angle was simulated by a sweep, and the results are shown in Fig. 10(b). As the angle of incidence only changes from 0 to 60 degrees, the absorption bandwidth and the position of the absorption peak remain nearly unchanged. It means that the structure is still able to work stably. In summary, the proposed metasurface-enhanced detector has the characteristics of polarization insensitivity and incidence angle insensitivity.

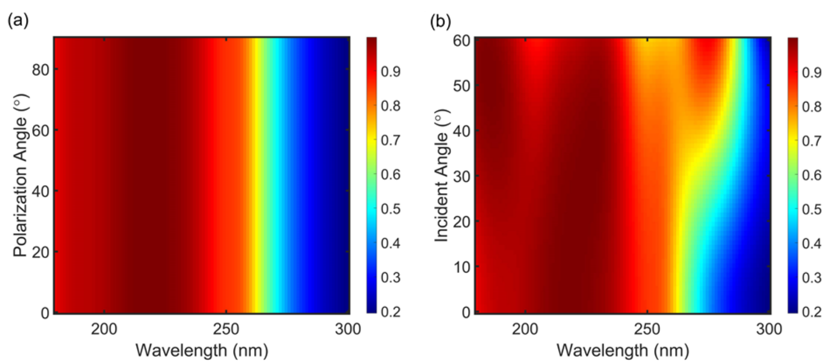

Fig. 10. Effect of polarization angle on absorption; (b) The effect of the angle of incidence on absorption

4. Conclusion

In this paper, an enhanced gallium oxide detector based on a diamond metasurface is proposed. Through the combination of Mie's resonance on the diamond metasurface, intrinsic absorption of gallium oxide, and metal mirror, the absorption rate of more than 90% in the solar blind ultraviolet band of 200-220 nm is achieved. The thickness of the required gallium oxide film is reduced to 20 nm. The carrier generation rate is 6 times the initial structure, improving detector responsiveness. The proposed metasurface structure can change its working wavelength by adjusting the geometric parameters and is polarization angle insensitive and incidence angle insensitive. Our results demonstrate the great potential of all-dielectric diamond metasurfaces for enhanced ultraviolet photoelectric conversion applications, which are expected to provide new economic relief solutions for applications such as ultraviolet detection, imaging, and communications.

Funding. The Science Fund for Distinguished Young Scholars of Jilin Province (20230101351JC); Scientific and Technological Development Project of Jilin Province (20220201080GX); National Natural Science Foundation of China (61735018); Excellent Member of Youth Innovation Promotion Association of the Chinese Academy of Sciences (Y201836); Leading Talents and Team Project of Scientific and Technological Innovation for Young and Middle-aged Groups in Jilin Province (20190101012JH); .

Disclosures. The authors declare no conflicts of interest.

Data availability. Data underlying the results presented in this paper are not publicly available at this time but may be obtained from the authors upon reasonable request.

References

1. H. Chen, H. Liu, Z. Zhang, K. Hu, and X. Fang, "Nanostructured Photodetectors: From Ultraviolet to Terahertz," Adv. Mater. **28**(3), 403–433 (2016).
2. X. Chen, F. Ren, S. Gu, and J. Ye, "Review of gallium-oxide-based solar-blind ultraviolet photodetectors," Photonics Res. **7**(4), 381–415 (2019).
3. M. Kumar, J.-Y. Park, and H. Seo, "High-Performance and Self-Powered Alternating Current Ultraviolet Photodetector for Digital Communication," ACS Appl. Mater. Interfaces **13**(10), 12241–12249 (2021).
4. L. Shi, K. Chen, A. Zhai, G. Li, M. Fan, Y. Hao, F. Zhu, H. Zhang, and Y. Cui, "Status and Outlook of Metal–Inorganic Semiconductor–Metal Photodetectors," Laser Photonics Rev. **15**(1), 2000401 (2021).
5. R. A. Ismail, A. M. Alwan, and A. S. Ahmed, "Preparation and characteristics study of nano-porous silicon UV photodetector," Appl. Nanosci. **7**(1-2), 9–15 (2017).
6. N. Nasiri, D. Jin, and A. Tricoli, "Nanoarchitechtonics of Visible-Blind Ultraviolet Photodetector Materials: Critical Features and Nano-Microfabrication," Adv. Opt. Mater. **7**(2), 1800580 (2019).
7. K. Nozaki, S. Matsuo, T. Fujii, K. Takeda, M. Ono, A. Shakoor, E. Kuramochi, and M. Notomi, "Photonic-crystal nano-photodetector with ultrasmall capacitance for on-chip light-to-voltage conversion without an amplifier," Optica **3**(5), 483–492 (2016).
8. C. Xie, X. T. Lu, X. W. Tong, Z. X. Zhang, F. X. Liang, L. Liang, L. B. Luo, and Y. C. Wu, "Recent Progress in Solar-Blind Deep-Ultraviolet Photodetectors Based on Inorganic Ultrawide Bandgap Semiconductors," Adv. Funct. Mater. **29**(9), 1806006 (2019).
9. J. Li, J. Li, S. Zhou, and F. Yi, "Metasurface Photodetectors," Micromachines **12**(12), 1584 (2021).
10. J. Hu, S. Bandyopadhyay, Y.-h. Liu, and L.-y. Shao, "A Review on Metasurface: From Principle to Smart Metadevices," Front. Phys. **8**, 586087 (2021).
11. C. Zhang, S. Divitt, Q. Fan, W. Zhu, A. Agrawal, Y. Lu, T. Xu, and H. J. Lezec, "Low-loss metasurface optics down to the deep ultraviolet region," Light: Sci. Appl. **9**(1), 55 (2020).
12. L. Chen, F. J. Ye, M. Cuo, S. S. Luo, J. J. Hao, Y. Ruan, and H. Y. Cui, "Ultraviolet-sensing metasurface for programmable electromagnetic scattering field manipulation by combining light control with a microwave field," Opt. Express **30**(11), 19212–19221 (2022).
13. K. Yao and Y. Zheng, "Near-ultraviolet dielectric metasurfaces: from surface-enhanced circular dichroism spectroscopy to polarization-preserving mirrors," J. Phys. Chem. C **123**(18), 11814–11822 (2019).
14. D. Zhao, Z. Lin, W. Zhu, H. J. Lezec, T. Xu, A. Agrawal, C. Zhang, and K. Huang, "Recent advances in ultraviolet nanophotonics: from plasmonics and metamaterials to metasurfaces," Nanophotonics **10**(9), 2283–2308 (2021).
15. T. Phan, D. Sell, E. W. Wang, S. Doshay, K. Edee, J. Yang, and J. A. Fan, "High-efficiency, large-area, topology-optimized metasurfaces," Light: Sci. Appl. **8**(1), 48 (2019).
16. M. Khorasaninejad, W. T. Chen, R. C. Devlin, J. Oh, A. Y. Zhu, and F. Capasso, "Metalenses at visible wavelengths: Diffraction-limited focusing and subwavelength resolution imaging," Science **352**(6290), 1190–1194 (2016).
17. W. T. Chen, M. Khorasaninejad, A. Y. Zhu, J. Oh, R. C. Devlin, A. Zaidi, and F. Capasso, "Generation of wavelength-independent subwavelength Bessel beams using metasurfaces," Light: Sci. Appl. **6**, e16259 (2017).
18. Q. Fan, W. Zhu, Y. Liang, P. Huo, C. Zhang, A. Agrawal, K. Huang, X. Luo, Y. Lu, C. Qiu, H. J. Lezec, and T. Xu, "Broadband Generation of Photonic Spin-Controlled Arbitrary Accelerating Light Beams in the Visible," Nano Lett. **19**(2), 1158–1165 (2019).
19. L. Huang, S. Zhang, and T. Zentgraf, "Metasurface holography: from fundamentals to applications," Nanophotonics **7**(6), 1169–1190 (2018).
20. A. C. Overvig, S. Shrestha, S. C. Malek, M. Lu, A. Stein, C. Zheng, and N. Yu, "Dielectric metasurfaces for complete and independent control of the optical amplitude and phase," Light: Sci. Appl. **8**(1), 92 (2019).
21. X. Chang, Y.-F. Wang, H. N. Abbasi, R. Wang, Z. Liu, J. Wang, W. Song, G. Chen, M. Zhang, W. Wang, K. Wang, and H.-X. Wang, "Pd nanoparticle size effects in localized surface plasmon-enhanced diamond photodetectors," Opt. Mater. **107**, 110031 (2020).
22. X. Cheng and Y. Wang, "Enhanced ultraviolet absorption in graphene by aluminum and magnesium hole-arrays," Sci. Rep. **11**(1), 8516 (2021).
23. A. Ghosh, S. M. M. Dhar Dwivedi, H. Ghadi, P. Chinnamuthu, S. Chakrabarti, and A. Mondal, "Boosted UV Sensitivity of Er-Doped In2O3 Thin Films Using Plasmonic Ag Nanoparticle-Based Surface Texturing," Plasmonics **13**(3), 1105–1113 (2018).
24. S. Han, H. Xia, Y. Lu, S. Hu, D. Zhang, W. Xu, M. Fang, W. Liu, P. Cao, and D. Zhu, "Great Enhancement Effect of 20-40 nm Ag NPs on Solar-Blind UV Response of the Mixed-Phase MgZnO Detector," ACS Omega **6**(10), 6699–6707 (2021).
25. K. Shimanoe, S. Endo, T. Matsuyama, K. Wada, and K. Okamoto, "Localized surface plasmon resonance in deep ultraviolet region below 200 nm using a nanohemisphere on mirror structure," Sci. Rep. **11**(1), 5169 (2021).
26. K. Teker, A. Hocaoglu, and M. A. Yildirim, "Improving detectivity of self-powered GaN ultraviolet photodetector by nickel nanoparticles," Appl. Phys. B **127**, 7 (2021).

27. J. Yu, J. Lou, Z. Wang, S. Ji, J. Chen, M. Yu, B. Peng, Y. Hu, L. Yuan, Y. Zhang, and R. Jia, “Surface modification of β-Ga2O3 layer using pt nanoparticles for improved deep UV photodetector performance,” J. Alloys Compd. **872**, 159508 (2021).
28. J. Yu, H.-J. Men, J.-W. Zhang, X.-W. Zhang, and N. Tian, “Design of a Surface Plasmon Resonance-Enhanced ZnO Ultraviolet Photodetector Based on a Sub-wavelength Metal Grating Covered with a High-Refractive-Index Medium,” J. Electron. Mater. **49**(8), 4469–4473 (2020).
29. R. Tang, G. Li, C. Li, J. Li, Y. Zhang, K. Huang, J. Ye, J. Kang, R. Zhang, and Y. Zheng, “Localized surface plasmon enhanced Ga 2 O 3 solar blind photodetectors,” Opt. Express **28**(4), 5731–5740 (2020).
30. G. M. Akselrod, J. Huang, T. B. Hoang, P. T. Bowen, L. Su, D. R. Smith, and M. H. Mikkelsen, “Large-Area Metasurface Perfect Absorbers from Visible to Near-Infrared,” Adv. Mater. **27**(48), 8028–8034 (2015).
31. C. Chen, Y. Liu, Z. Y. Jiang, C. Shen, Y. Zhang, F. Zhong, L. Chen, S. Zhu, and H. Liu, “Large-area long-wave infrared broadband all-dielectric metasurface absorber based on markless laser direct writing lithography,” Opt. Express **30**(8), 13391–13403 (2022).
32. J. He, C. Y. Li, D. X. Qi, Q. Cai, Y. Liu, R. H. Fan, J. Su, P. Huo, T. Xu, R. Peng, and M. Wang, “Improving Photoelectric Conversion with Broadband Perovskite Metasurface,” Nano Lett. **22**(16), 6655–6663 (2022).
33. X. Liu, K. Fan, I. V. Shadrivov, and W. J. Padilla, “Experimental realization of a terahertz all-dielectric metasurface absorber,” Opt. Express **25**(1), 191–201 (2017).
34. S. Song, Q. Chen, L. Jin, and F. Sun, “Great light absorption enhancement in a graphene photodetector integrated with a metamaterial perfect absorber,” Nanoscale **5**(20), 9615–9619 (2013).
35. C.-Y. Yang, J.-H. Yang, Z.-Y. Yang, Z.-X. Zhou, M.-G. Sun, V. E. Babicheva, and K.-P. Chen, “Nonradiating Silicon Nanoantenna Metasurfaces as Narrowband Absorbers,” ACS Photonics **5**(7), 2596–2601 (2018).
36. J. Yang, Z. Zhu, J. Zhang, W. Xu, C. Guo, K. Liu, M. Zhu, H. Chen, R. Zhang, X. Yuan, and S. Qin, “Mie resonance induced broadband near-perfect absorption in nonstructured graphene loaded with periodical dielectric wires,” Opt. Express **26**(16), 20174–20182 (2018).
37. Z. X. Zhou, M. J. Ye, M. W. Yu, J. H. Yang, K. L. Su, C. C. Yang, C. Y. Lin, V. E. Babicheva, I. V. Timofeev, and K. P. Chen, “Germanium Metasurfaces with Lattice Kerker Effect in Near-Infrared Photodetectors,” ACS Nano **16**(4), 5994–6001 (2022).
38. J. Xu, W. Zheng, and F. Huang, “Gallium oxide solar-blind ultraviolet photodetectors: a review,” J. Mater. Chem. C **7**(29), 8753–8770 (2019).
39. C. Xie, X.-T. Lu, M.-R. Ma, X.-W. Tong, Z.-X. Zhang, L. Wang, C.-Y. Wu, W.-H. Yang, and L.-B. Luo, “Catalyst-Free Vapor–Solid Deposition Growth of β-Ga2O3 Nanowires for DUV Photodetector and Image Sensor Application,” Adv. Opt. Mater. **7**(24), 1901257 (2019).
40. M. Kim, J.-H. Seo, U. Singisetti, and Z. Ma, “Recent advances in free-standing single crystalline wide band-gap semiconductors and their applications: GaN, SiC, ZnO, β-Ga2O3, and diamond,” J. Mater. Chem. C **5**(33), 8338–8354 (2017).
41. S. Kossar, R. Amiruddin, and A. Rasool, “Study on thickness-dependence characteristics of bismuth ferrite (BFO) for ultraviolet (UV) photodetector application,” Micro and Nano Syst. Lett. **9**(1), 1 (2021).
42. T.-Y. Huang, R. R. Grote, S. A. Mann, D. A. Hopper, A. L. Exarhos, G. G. Lopez, A. R. Klein, E. C. Garnett, and L. C. Bassett, “A monolithic immersion metalens for imaging solid-state quantum emitters,” Nat. Commun. **10**(1), 2392 (2019).
43. J. L. Zhang, K. G. Lagoudakis, Y.-K. Tzeng, C. Dory, M. Radulaski, Y. Kelaita, K. A. Fischer, S. Sun, Z.-X. Shen, N. A. Melosh, S. Chu, and J. Vučković, “Complete coherent control of silicon vacancies in diamond nanopillars containing single defect centers,” Optica **4**(11), 1317–1321 (2017).
44. I. H. Malitson, “Interspecimen comparison of the refractive index of fused silica,” J. Opt. Soc. Am. **55**(10), 1205–1209 (1965).
45. A. Paskaleva, D. Spassov, and P. Terziyska, “Electric, dielectric and optical properties of Ga2O3 grown by metal organic chemical vapour deposition,” in *Journal of Physics: Conference Series*, (IOP Publishing, 2017), 012017.
46. H. Phillip and E. Taft, “Kramers-Kronig analysis of reflectance data for diamond,” Phys. Rev. **136**(5A), A1445–A1448 (1964).
47. A. D. Rakić, “Algorithm for the determination of intrinsic optical constants of metal films: application to aluminum,” Appl. Opt. **34**(22), 4755–4767 (1995).
48. J. Hu, B. Xu, Z. Zhang, X. He, L. Li, H. Cheng, J. Wang, J. Meng, X. Wang, and C. Zhang, “Step flow growth of β-Ga2O3 films on off-axis 4H-SiC substrates by LPCVD,” Surf. Interfaces **37**, 102732 (2023).
49. M. Higashiwaki, “MBE growth and device applications of Ga2O3,” *Molecular Beam Epitaxy: Materials and Applications for Electronics and Optoelectronics* 411–422 (2019).
50. N. Blumenschein, T. Paskova, and J. F. Muth, “Effect of growth pressure on PLD-deposited gallium oxide thin films for deep-UV photodetectors,” Phys. Status Solidi A **216**(20), 1900098 (2019).
51. Y. Yang, W. Liu, T. Huang, M. Qiu, R. Zhang, W. Yang, J. He, X. Chen, and N. Dai, “Low deposition temperature amorphous ALD-Ga2O3 thin films and decoration with MoS2 multilayers toward flexible solar-blind photodetectors,” ACS Appl. Mater. Interfaces **13**(35), 41802–41809 (2021).
52. Y. J. Lu, C. N. Lin, and C. X. Shan, “Optoelectronic diamond: growth, properties, and photodetection applications,” Adv. Opt. Mater. **6**(20), 1800359 (2018).

Optics EXPRESS

53. M. Malakoutian, Y. Song, C. Yuan, C. Ren, J. S. Lundh, R. M. Lavelle, J. E. Brown, D. W. Snyder, S. Graham, and S. Choi, "Polycrystalline diamond growth on β-Ga2O3 for thermal management," Appl. Phys. Express **14**(5), 055502 (2021).
54. K. Li, J. Zang, X. Yang, Y. Tian, C. Lin, P. Sun, Z. Zhang, Y. Chen, and C. Shan, "Solar-Blind Position-Sensitive Detectors Fabricated from β-Ga2O3/Polycrystalline Diamond Heterojunctions," Phys. Status Solidi RRL **15**(10), 2100347 (2021).
55. S. Modak, J. S. Lundh, N. S. Al-Mamun, L. Chernyak, A. Haque, T. Q. Tu, A. Kuramata, M. J. Tadjer, and S. J. Pearton, "Growth and characterization of α-Ga2O3 on sapphire and nanocrystalline β-Ga2O3 on diamond substrates by halide vapor phase epitaxy," J. Vac. Sci. Technol., A **40**(6), 062703 (2022).
56. Z. Cheng, V. D. Wheeler, T. Bai, J. Shi, M. J. Tadjer, T. Feygelson, K. D. Hobart, M. S. Goorsky, and S. Graham, "Integration of polycrystalline Ga2O3 on diamond for thermal management," Appl. Phys. Lett. **116**(6), 062105 (2020).
57. M. Decker, I. Staude, M. Falkner, J. Dominguez, D. N. Neshev, I. Brener, T. Pertsch, and Y. S. Kivshar, "High-Efficiency Dielectric Huygens' Surfaces," Adv. Opt. Mater. **3**(6), 813–820 (2015).